AIAA JOURNAL
Vol. 43, No. 2, February 2005

Numerical Investigation of Reflected Shock/Vortex Interaction near an Open-Ended Duct

Shen-Min Liang,* Wen-Tai Chung,† and Hua Chen‡
National Cheng Kung University, Tainan 701, Taiwan, Republic of China
and
Shiuh-Hwa Shyu§
Wu-Feng Institute of Technology, Chia-I 621, Taiwan, Republic of China

The problem of planar reflected-shock/spiral-vortex interactions near an open-ended duct is considered. The reflected shock is formed after exiting the duct and impinging on a vertical wall that is located downstream of the duct. Two cases associated with the shock diffraction around the duct exit are investigated for understanding the detailed flow structure and acoustic waves due to the reflected shock/spiral-vortex interaction. One is a 90-deg diffraction; the other is a 180-deg diffraction. An Euler solver with a high-resolution scheme of weighted essential nonoscillation is used to study these complicated flow problems. The Euler solver is validated to be reasonably accurate by comparing the computed solution with experimental data. For the study of reflected-shock/spiral-vortex interactions, the techniques of computational shadowgraph, computational schlieren image, and computational interferometry are used. Detailed flow structures of reflected shock/vortex interactions are reported for different incident shock Mach numbers. An interesting result of stagnant reflected shock waves downstream of the duct is found for an incident shock Mach number equal to or greater than 1.4. For the incident shock Mach number below this critical value, the reflected shock R_1 will eventually enter the duct. The mechanism for the formation of acoustic waves generated by reflected-shock/vortex interactions is analyzed.

I. Introduction

A SHOCK/VORTEX interaction is an interesting and complicated problem, and its associated noise is important for engineers and scientists because the noise reduction problem in environmental protection issues has been stressed in the past 10 years. In this study, a planar shock wave, which is discharged from a two-dimensional duct and then impinges on a downstream vertical wall, is considered. When the shock wave diffracts around the 90-deg sharp corner at the duct exit, vortices downstream of the duct are induced. Subsequently, the induced vortices will interact with the reflected shock wave, which is the primary shock wave reflected from the vertical wall. The reflected shock/vortex interaction is very complicated, resulting in noise. Thus, the purpose of this study is to investigate numerically the detailed flow structure due to the reflected shock/vortex interaction and to try to understand its mechanism of noise generation. This basic study would be helpful for understanding a three-dimensional shock/vortex interaction in real problems and serves as a stepping-stone for engineering applications on noise reduction, such as in exhaust pipes for automobiles.

Over the past 30 years, there have a great number of papers that are directly or indirectly related to shock/vortex interactions. We have not attempted to review all papers because of space limitations. Skews[1] reported his experimental results of basic flow and wave structures behind a shock wave diffracting around plane-walled convex corners. In the perturbed region, there are expansion waves, a slipstream, an induced spiral vortex, a contact surface, and a second shock on the slipstream. Takayama and Inoue[2] collected some computational and experimental results for the problem of shock wave diffraction over a 90-deg sharp corner. In those results, a vortex shock across the induced spiral vortex and a second shock on the slipstream were numerically predicted and experimentally observed. Moreover, in the color schlieren photograph of Ritzerfeld et al.,[2] a series of second shock waves along the slipstream were also found. Yang et al.[3] used the holographic interferometry technique to observe the detailed flows induced by the shock waves diffracted around a 90-deg sharp corner. In addition to the holographic interferometry, schlieren and shadowgraph techniques are also useful for flow visualization. Yates[4] presented interferograms, schlieren images, and shadowgraphs constructed from computed flowfields for flow problems that include a ramp flow, a blunt-body flow, a nozzle flow, and a reacting flow. From these images, one could clearly see flow structures with discontinuities. These three flow visualization techniques provide useful tools for analyzing computational data obtained from numerical simulation, in particular, for the present problem of shock/vortex interaction and its associated acoustic waves. Sun and Takayama[5] experimentally and numerically studied the problem of the formation of a second shock wave after shock wave diffraction around a sharp corner for an airstream. They found that the critical shock Mach number for the formation of the second shock is 1.346.

Kim and Setoguchi[6] experimentally and numerically investigated the downstream pressure variation of a shocked flow discharged from a shock tube with a circular baffle plate at the tube exit. The shock Mach number ranged from 1.02 to 1.45. For numerical simulation, they solved the Euler equations using a total-variation-diminishing scheme. They found that the baffle plate could strongly influence the pulse wave (noise) induced by the discharged shock wave when the diameter of the baffle plate is less than three times the duct diameter. Jiang and Takayama[7] proposed an image method for the construction of a flow structure from numerical solutions using an effective density integration algorithm. They obtained good agreement between experimental and numerical results based on characteristic flow structures and density differences. Szumowski et al.[8] experimentally and numerically investigated the interactions of starting jets and a downstream wall for flow Mach number ranging from 0.65 to 1.14. To study the problem, they used a schlieren

Received 11 May 2003; revision received 26 May 2004; accepted for publication 22 July 2004.

*Professor, Institute of Aeronautics and Astronautics. Associate Fellow AIAA.
†Graduate Student, Institute of Aeronautics and Astronautics.
‡Graduate Student, Institute of Aeronautics and Astronautics; currently Assistant Professor, Department of Information Communication, Leader University, Tainan 709, Taiwan, Republic of China.
§Assistant Professor, Department of Mechanical Engineering.

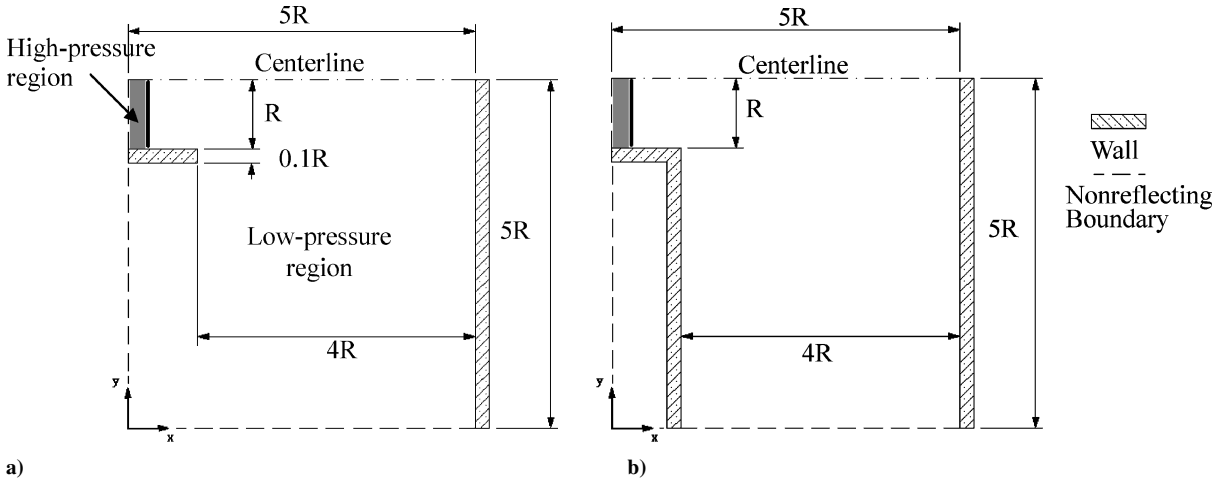

Fig. 1 Schematic of problems of interest and computational domain: a) 180-deg diffraction case and b) 90-deg diffraction case.

system for experimentation and the McCormack predictor–corrector scheme for the Euler solver and obtained good agreement between experimental and numerical results on the trajectories of the ring vortex plane and the shock and on the radii of the vortex ring at different instants. They also found impulsive sound waves that were generated by the shock/vortex interaction and by the vortex impact on the vertical wall. In particular, toroidal pressure pulses during the reflected-shock/ring-vortex interaction were found. Inoue and Hattori[9] numerically simulated shock/vortex interactions and found that the acoustic wave generated is of quadrupolar nature and that three sound waves are generated in a form of alternating compressions and rarefactions. Chen and Liang[10] investigated a planar blast/vortex interaction and its generated acoustic waves. They found four sound waves generated for a blast/vortex interaction. This result was contrasted to that for the corresponding shock/vortex interaction studied by Inoue and Hattori.[9] Very recently, Henderson et al.[11] numerically and analytically studied the wall-jetting effect in Mach reflection. In particular, a cascade of alternating rarefaction and compression waves, that is, a series of shock waves, along a slipstream was found. Sun and Takayama[12] studied the vorticity production due to shock diffraction around sharp corners and concluded that the slipstream is a more dominant factor for the vorticity production than baroclinic effects.

In this study, a high-resolution Euler solver is used to study the problem of reflected-shock/spiral-vortex interactions and their associated pulse waves. A spiral vortex induced by shock wave diffraction is more complicated than a plain vortex as used in Ref. 9 because of a slipstream in the spiral vortex. For spatial discretization, a fifth-order weighted essentially nonoscillation scheme of Jiang and Shu[13] is employed, and a fourth-order Runge–Kutta method is used for time integration. The working fluid is air. To analyze detailed flowfields, the computational techniques of shadowgraphs, schlieren images, and interferograms are used.

II. Problems of Interest and Numerical Method

Two problems of two-dimensional shocked duct flows considered in this study are schematically shown in Fig. 1. One is a duct with a baffle plate at its exit; the other is simply a duct with a wall thickness of $0.1R$. Both ducts have a width of $2R$. A vertical wall is located at a distance of 4R from the duct entrance. Inside the duct there is a planar right-moving shock wave at a Mach number M_s ranging from 1.2 to 2. The moving shock will propagate out of the duct and impinge on the downstream wall. Only a half domain, as shown in Fig. 1, is used for computation to save computational time and computer memory. Without the consideration of viscous effects, as done by Szumowski et al.,[8] the equations governing the flow are the Euler equations. The assumption of inviscid flow was validated by the experimental results of Szumowski et al.[8] and of Yang.[14] Yang found that the vortices induced by the shear layer are relatively small compared to the induced vortex due to a diffracted shock.

The Euler equations are nondimensionalized by flow conditions of the quiescent air ahead of the incident shock. The characteristic length is chosen to be a half-duct width R. The time variable t is normalized by the characteristic time R/c, where c is the speed of sound in the quiescent air ahead of the incident shock. The convective terms of the Euler equations are numerically discretized by a fifth-order weighted essentially nonoscillatory scheme of Jiang and Shu,[13] and a fourth-order Runge–Kutta scheme is used for time integration. Central differencing is used for viscous terms if viscous flow is considered. The boundary condition imposed on the duct and baffle plates is the slip condition for inviscid flow and the no-slip condition for viscous flow. On the centerline, a symmetry condition is prescribed. On the other boundaries, as indicated by the dashed line in Fig. 1, the nonreflecting boundary condition of Thompson[15] is prescribed. An incident shock wave is developed by the rupture of a diaphragm between a high-pressure region and a low-pressure region at an upstream position of the duct.

III. Results and Discussion

A. Code Validation

To validate the accuracy of our Euler solver, the axisymmetric problem of Szumowski et al.[8] is solved. This problem is to consider a moving shock wave that is discharged from a shock tube with a diameter of 65 mm and impinges on a downstream vertical wall located at a distance 130 mm from the tube. A particular case of shock Mach number equal to 1.2, producing a jet flow with a Mach number of 0.65, is further investigated here to understand the complicated wave structure of a reflected shock/vortex interaction by using our Euler and Navier–Stokes solvers. For viscous flow calculation, the flow is assumed to be laminar with a Reynolds number of 1×10^4. The computational domain is chosen to be as that shown in Fig. 1. Three uniform grids, 250×250 (coarse grid), 500×500 (intermediate grid), and 750×750 (fine grid), are used for the inviscid flow calculation, and a 1000×1000 grid is used for the viscous flow calculation. The Courant–Friedrichs–Lewy number (CFL) is chosen to be 0.6. It was found that the computed dimensionless pressure at the vortex center is 0.5 for the coarse grid, 0.365 for the intermediate grid, and 0.347 for the fine grid. It is clear that the coarse grid is not fine enough to obtain an accurate solution, and the intermediate-grid solution is as accurate as the fine-grid solution. Moreover, the computed flowfields at $t = 0.61$ for these three grids are almost the same, except for some small vortices along the slipstream for the fine-grid solution. Thus, we will use the intermediate grid for later study. Three different values of CFL, 0.4, 0.6, and 0.8, were tested to see the CFL effect on the numerical solution. The computed pressure at the vortex center on the intermediate grid is 0.366 for CFL = 0.4, 0.365 for CFL = 0.6, and 0.364 for CFL = 0.8. Clearly, CFL number has no significant effect on the numerical solution. Thus, the CFL is chosen to be 0.6 for the subsequent study.

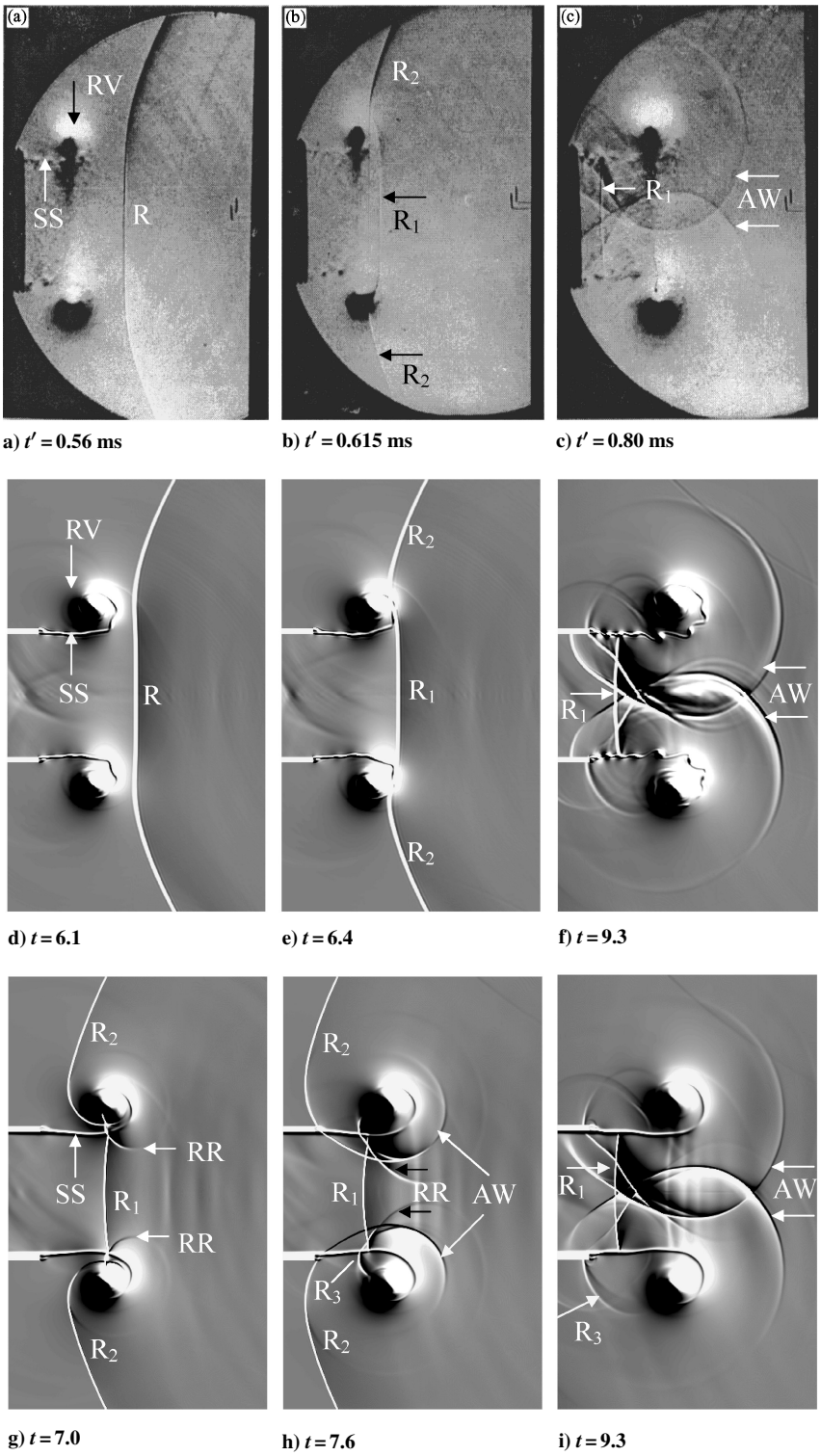

Fig. 2 Computational schlieren pictures of shock wave discharged from a circular duct at different instants, $M_s = 1.2$: a–c) experimental results,[8] d–f) Euler solutions, and g–i) Navier–Stokes solutions.

When the discharged shock wave leaves the tube, a ring vortex is induced behind it. This discharged shock wave will be reflected from the downstream wall and interact with the induced ring vortex. We will investigate the detailed flowfield of reflected-shock/ring-vortex interaction.

Our computed schlieren pictures at different instants are shown in Figs. 2d–2i and compared with experimental schlieren pictures of Szumowski et al.[8] as shown in Figs. 2a–2c. Figures 2d–2f show the Euler solutions, and Figs. 2g–2i the Navier–Stokes solutions. Figure 2a shows the flowfield of a circular-type slipstream (SS), an induced ring vortex (RV), and a reflected shock wave R from the downstream plate at $t' = 0.56$ ms after the incident shock wave leaves the tube. At this instant, the reflected shock wave is going to interact with the ring vortex. At $t' = 0.615$ ms, the reflected shock wave is interacting with the ring vortex. One can see that the reflected shock wave is distorted in shape due to the accelerating phase of rotating vortex on the shock wave, that is, the opposite flow direction as the moving shock wave. We basically split the reflected shock wave R into two parts: the undistorted wave R_1 and the distorted wave R_2 as shown in Fig. 2b. The undistorted wave retains a straight shape, and a curved shape develops for the distorted wave. Later, the reflected shock wave R_2 will be further distorted. At $t' = 0.8$ ms, the

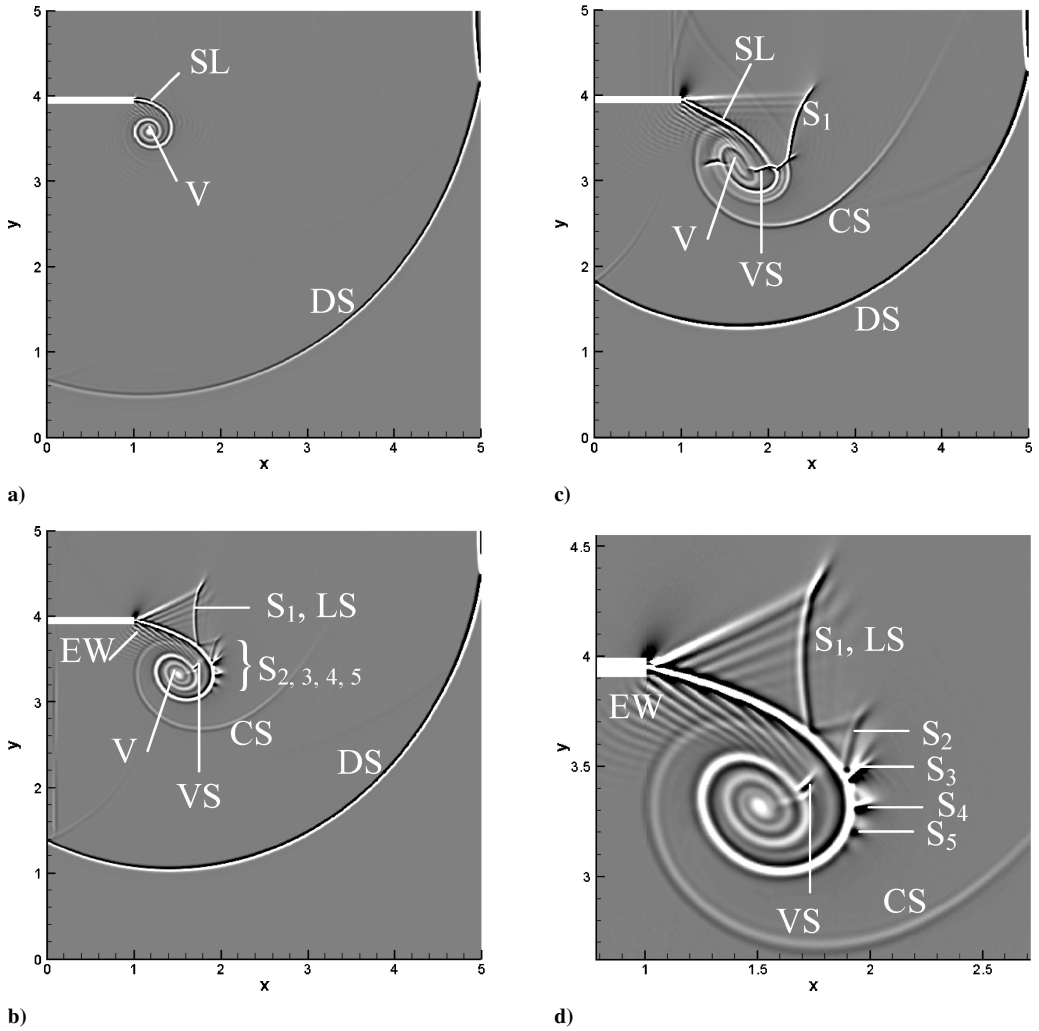

Fig. 3 Computational shadowgraphs of the local flowfield due to shock wave diffraction near the duct exit for different incident shock Mach numbers: a) $M_s = 1.2$, $t = 3.4$; b) $M_s = 1.6$, $t = 2.6$; c) $M_s = 2.0$, $t = 2.2$; and d) enlargement of induced vortex for $M_s = 1.6$ case.

reflected shock/vortex interaction has finished, resulting in a toroidal acoustic wave (AW). We will further investigate the formation of the toroidal AW because Szumowski et al. did not explore this point. By comparing Figs. 2a–2c with Figs. 2d–2f, we can see that both the computed and experimental wave patterns agree quite well. We also compare our Navier–Stokes solution with the Euler solutions. It is found that no significant difference was found between these two solutions, except for the SS shape. In the Euler solution, the SS develops a wavy shape because of the Kelvin–Helmholtz instability, but a smooth SS shape for the Navier–Stokes solution. This difference can be seen in Figs. 2f and 2i.

To see the evolution of the reflected-shock/vortex interaction, we only plot the wave patterns of the Navier–Stokes solutions at $t = 7.0$, 7.6, and 9.3. At $t = 7.0$, the reflected shock wave R_2 has almost finished the interaction with the ring vortex, and is leaving the ring vortex. The R_1 shock that penetrates the core of the RV produces a toroidal reflected wave (denoted by RR), issuing from the SS. The intermediate reflected shockwave R_3 between the outer and inner SSs will grow into a curved shock wave. At $t = 7.6$ and 9.3, the R_2 shock almost reaches the duct, the R_1 shock moving closer to the duct, and the toroidal AW is well developed, as shown in Figs. 2h and 2i From Figs. 2h and 2i, we conclude that the toroidal sound wave results from the diffraction of the reflected shock wave R_2 around the RV.

In addition to the qualitative comparison, a quantitative comparison is made by checking the wall shock Mach number for a plain problem of shock diffraction around a 90-deg sharp (expansion) corner. Two cases of $M_s = 1.5$ and 2.0 are considered. The computed values of wall shock Mach number are 1.12 and 1.26, respectively, which agree very well with the experimental data of 1.15 and 1.26 in Ref. 16. The relative errors are 2.5 and 3.1%, respectively.

B. Problem of Reflected Shock/Vortex Interaction

Case 1:180-Degree Diffraction

In this case, the flow problem is in Fig. 1a. With the characteristic length of the half duct width R, the computational domain after normalization is $\{(x, y)|0 \le x \le 5, 0 \le y \le 5\}$. The initial shock wave is located at $x = 0.1$. The computational grid consists of 500×500 grid points.

When the incident shock wave arrives at the duct exit, it diffracts around the 180-deg corner, resulting in an induced spiral vortex in the half computational domain. Figure 3 shows the computational shadowgraphs at different instants for different incident shock Mach numbers. For the weak shock wave case of $M_s = 1.2$, at $t = 3.4$, the incident shock reaches the downstream wall. The slipline (SL), the induced spiral vortex V, and the diffracted shock (DS) are clearly shown in Fig. 3a. Some expansive waves along the SL may exist, but are not clearly seen in Fig. 3a. For the $M_s = 1.6$ case, at $t = 2.6$, more waves are generated in addition to the SL, the contact surface (CS), and the spiral vortex. There are a series of secondary shock waves, S_1, S_2, S_3, S_4, and S_5, a vortex shock (VS), and some associated expansive waves (EW) along the SL, as shown in Fig. 3b. An enlarged plot showing these waves is given in Fig. 3d. The VS is not clearly seen in this case. The existence of the EW causes the local flow to accelerate to supersonic speed along the upstream SL, resulting in the formation of a series of shock waves, called a shock train. This shock train phenomenon was also experimentally

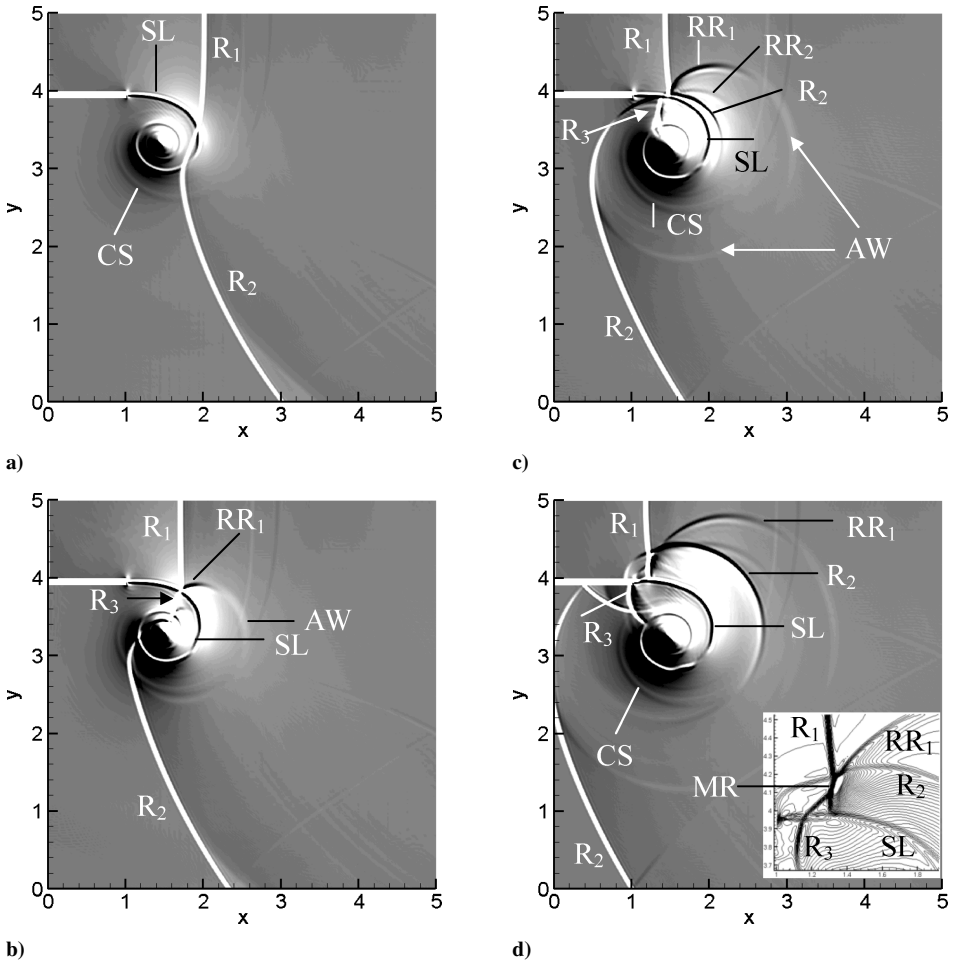

Fig. 4 Computational schlieren images of reflected shock/spiral-vortex interaction for different instants, $M_s = 1.2$: a) $t = 6.7$; b) $t = 7.2$; c) $t = 7.7$; and d) $t = 8.2$.

observed by Yang[14] and by Kleine et al.[17] The first shock S_1 was sometimes referred as a lambda shock (LS).[17] This is locally very similar to a shock train existing in internal gas flows.[18] Later on, the main secondary shock wave S_1 survives, and the other secondary shocks disappear. This implies that the flow is not self-similar at later times because of the effect of finite duct width. For a stronger shock wave of $M_s = 2.0$, only the secondary shock wave S_1 and a VS wave are generated, as shown in Fig. 3c. The present result is consistent with the experimental result of Kleine et al.[17] for $M_s = 1.45$–1.85.

Figure 4 shows the flowfields during and after the reflected-shock/vortex interactions for $t = 6.7$–8.2 and $M_s = 1.2$. Figures 4a–4d show the computational schlieren images at different instants. At $t = 6.7$, the reflected shock R starts to interact with the induced vortex and is slightly distorted by the vortex, as shown in Figs. 4a. We divide the reflected shock R into two parts: the upper part R_1 and the lower part R_2. At this moment, the reflected shock has not passed through the vortex center, and the dimensionless pressure at the vortex center is as low as 0.417 compared to the dimensionless pressure of unity of the undisturbed air. At $t = 7.2$, the reflected shocks R_1 and R_2 are interacting with the vortex, as shown in Fig. 4b, and are separated by the intermediate shock R_3 between the outer and inner SLs. Because of the reflected shock R_1 penetrating the spiral SL, two visible weaker rereflected shocks (RR_1 and RR_2) result. The shock (RR_1) is a rereflected wave induced by the outer SL and the RR_2 shock by the inner SL. Because the reflected shock R_2 has passed the vortex center, the corresponding pressure at the vortex center is increased to 0.468. A very weak compressive wave, an AW, is generated, connecting with the rereflected shock (RR_1). At $t = 7.7$, the reflected shock R_2 leaves the spiral vortex, and moves close to the duct wall. At the same time, the R_2 wave penetrates the outer SL. The dimensionless pressure at the vortex center is decreased to 0.446 because of the movement of the R_2 shock away from the spiral vortex. At $t = 8.2$, the basic wave structure, as shown in Fig. 4d, is very similar to that in Fig. 4c, except for the reflected shock R_1 moving closer to the duct. With the growth of the R_3 wave, a Mach reflection is developed, as shown in the inset. This wave pattern of Mach reflection illustrates the complicated interaction of the R_1, R_2, R_3, and RR_1 waves. At this instant, the dimensionless pressure at the vortex center is slightly decreased to 0.44.

For the cases of $M_s = 1.6$ and 2.0, the basic wave structures due to the reflected-shock/vortex interactions are similar to that in Fig. 4 for the $M_s = 1.2$ case. The dimensionless pressure variations before and after the passage of the reflected shock through the vortex for different incident shock Mach numbers are shown in Fig. 5. One can see that the vortex center pressure is rapidly decreased when Mach number M_s is increased from 1.1 to 1.6, but it is not significantly changed when Mach number M_s is increased from 1.6 to 2. The reason is that, for $M_s < 1.6$, there is enough time required for a full development of the spiral vortex before the passage of the reflected shock. For $M_s \geq 1.6$, the time for the development of the spiral vortex is very short before the passage of the reflected shock. The stronger the incident shock, the shorter the time is for the spiral vortex development before the reflected shock passing through the spiral vortex. Thus, for $M_s < 1.6$, the stronger the incident shock, stronger is the spiral vortex and the lower the vortex center pressure. For $1.6 \leq M_s \leq 2.0$, because the spiral vortex is still in its infant stage, the (dimensionless) vortex center pressure is as low as about 0.1 before the passage of the reflected shock. After the passage of the reflected shock wave, the vortex center pressure is abruptly increased. The abrupt pressure increase is believed to be due to the baroclinic effect that is the misalignment of the pressure and density gradients.

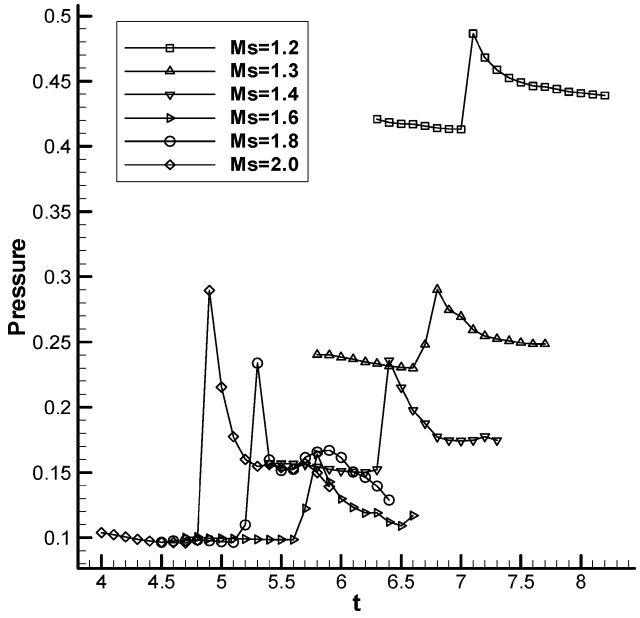

Fig. 5 Pressure variations at the vortex center for different incident shock Mach numbers.

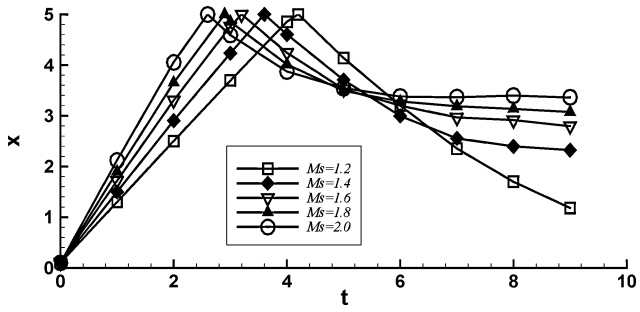

Fig. 6 Positions of the reflected shock waves for different incident shock Mach numbers.

Another interesting result is the whereabouts of the reflected shock wave R_1 for long times. Figure 6 shows the locations of the incident and reflected shocks vs the dimensionless time for different incident shock Mach numbers. It is clearly seen that the incident shock location is increased linearly with time because of a constant shock speed before $x = 5$, where the downstream wall is located, for $M_s = 1.2$–2.0. One can see that the position of the reflected shock R_1 decreases with time for $M_s < 1.4$ and tends to a constant for $M_s \geq 1.4$. We plotted the position of the reflected shock R_1 for $t > 9$. It was found that the reflected shock R_1 eventually enters the duct for $M_s < 1.4$, and for $M_s \geq 1.4$, the R_1 shock almost stays stagnant outside the duct with a slight oscillation because of the movement of the spiral vortex. The critical value of shock Mach number M_s for a stagnant reflected shock staying outside the duct is roughly about 1.4. The corresponding distance, x_{cr}, is approximately $x_{cr} = 2.65$, which is a distance of 1.65 R downstream from the duct exit. For shock Mach number M_s greater than the critical value, the reflected shock R_1 will stay at the location farther upstream of the critical value, x_{cr}.

Figure 7 shows the computational interferograms for $M_s = 1.2$, 1.6, and 2.0 at $t = 8.0$, 6.9, and 6.1, respectively. The density increment for each case is indicated. The SL, the reflected shocks R_1 and R_2, and the CS are also indicated. The CS in the case of $M_s = 1.2$ is not clearly seen in Fig. 7a because the incident shock is weak, unlike in other two cases. In this case, no second shock is formed. However, for the other two cases, a second shock S_1 is developed, behind the reflected shock R_1, as shown in Figs. 7b and 7c. Note that, as mentioned with reference to Fig. 3b, this second shock is developed above the upstream SL in earlier time. For $M_s = 1.2$, the dimensionless density right before the reflected shock R_1, as shown in Fig. 7a, is 0.979. This value is greater than the critical density ratio, 0.851, of an isentropic flow. This means that the flow before the reflected shock R_1 is subsonic so that the R_1 shock can propagate into the duct. For the $M_s = 1.6$ and 2.0 cases, the dimensionless densities right before the R_1 shock are 0.598 and 0.817, respectively. These two values are less than the critical density ratios, 1.288 and 1.679, for an isentropic flow, respectively. This implies that the flow before the reflected shock R_1 is supersonic, resulting in a stagnant shock outside the duct, as shown in Figs. 7b and 7c. Moreover, from Fig. 7c we can see some small vortices induced by the contact surface. The reason for the formation of these small vortices V_1 is unknown yet, and thus, further investigation is needed.

Case 2: 90-Degree Diffraction

In this case, the main difference from the first case is the double passage of the R_2 shock through the spiral vortex. We only

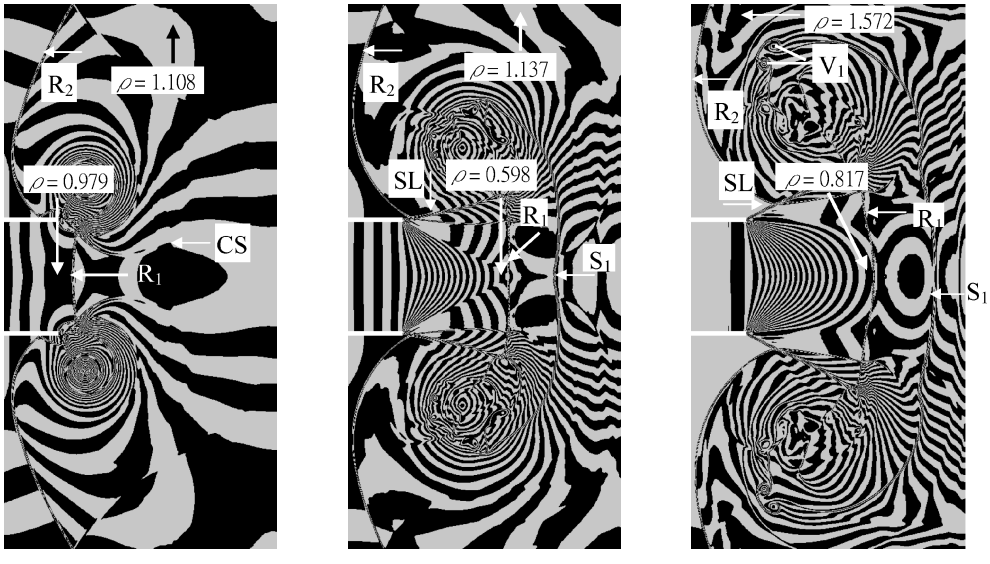

a) b) c)

Fig. 7 Computational holographic interferograms of flowfields for different incident Mach numbers: a) $M_s = 1.2$, $t = 8.0$, $\Delta\rho = 7.67 \times 10^{-3}$; b) $M_s = 1.6$, $t = 6.9$, $\Delta\rho = 3.65 \times 10^{-2}$; and c) $M_s = 2.0$, $t = 6.1$, $\Delta\rho = 5.39 \times 10^{-2}$.

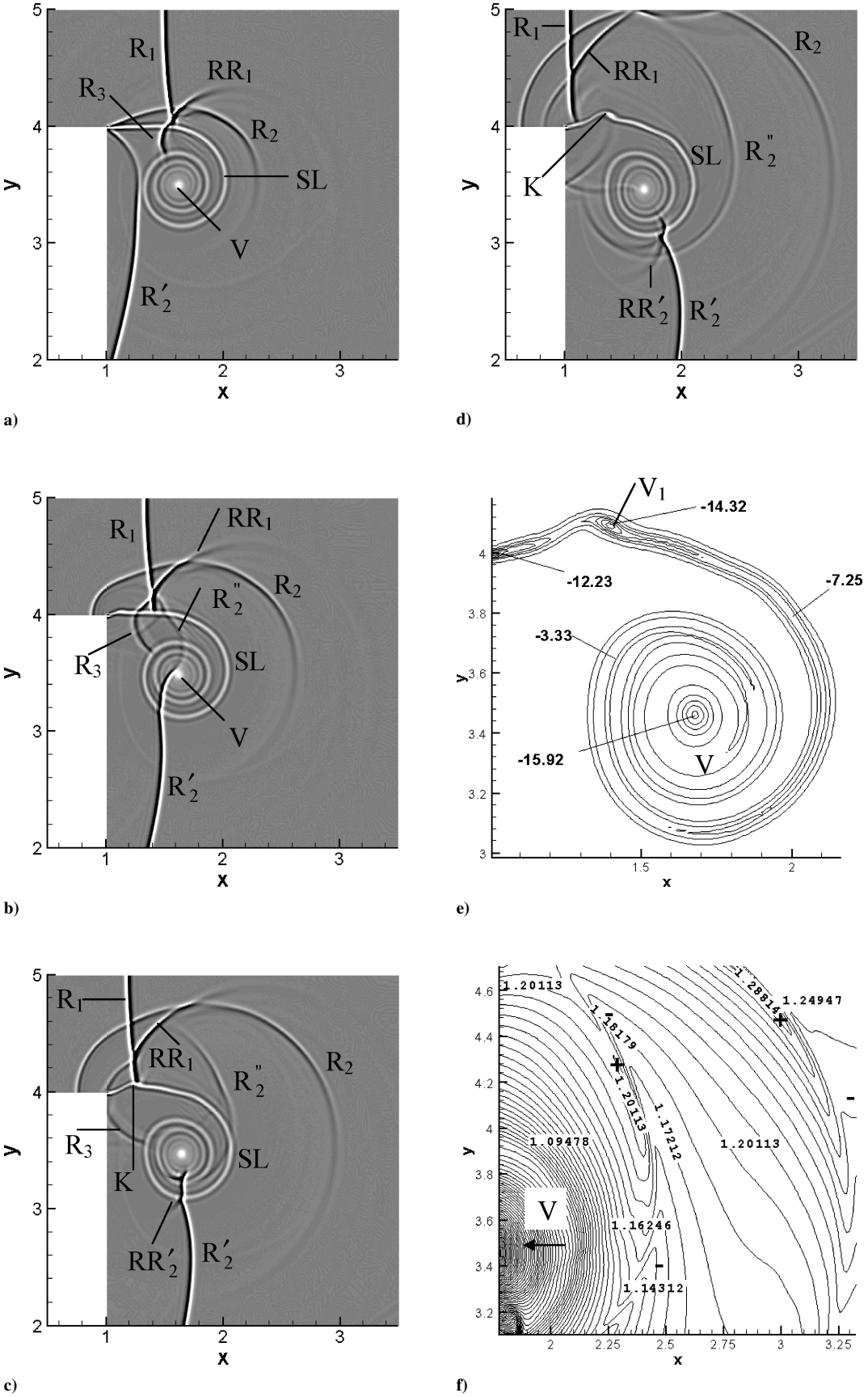

Fig. 8 Computational shadowgraphs of local flowfields at different instants for the case of 90-deg shock diffraction; $M_s = 1.2$: a) $t = 7.6$, b) $t = 7.9$, c) $t = 8.2$, d) $t = 8.5$, e) enlarged plot of vorticity distribution for spiral vortex V, and f) corresponding pressure distribution in a prescribed region (R, reflected shock; R'_2, reflected shock from wall; RR, rereflected shock from slip line; SL, slip line; and V, spiral vortex).

concentrate on the study of the second shock/vortex interaction. Figure 8 shows the shadowgraphs of the second shock/vortex interaction at different instants for $M_s = 1.2$. At $t = 7.6$, the original reflected shock R_2 is reflected from the left wall and is denoted R_2', as shown in Fig. 8a. The R_2' shock connects the R_2 shock at the duct corner. Thus, the SL is greatly perturbed. The R_2' shock starts to interact with the spiral vortex V. At $t = 7.9$, the R_2' shock interacts with the spiral vortex V, causing its shape distortion, as shown in Fig. 8b. The upper part of the R_2' shock above the vortex center is denoted R_2'' and is accelerated by the spiral vortex downstream. The R_2 shock moves further upstream and enters the duct. At $t = 8.2$, a kink K on the SL is formed, which will develop into a vortex. Because of the penetration of the R_2' shock through the SL, a reflection wave RR_2' is issued from the SL, as shown in Fig. 8c. The intermediate shock R_3 between the outer and inner SLs, impinges on the wall and will reflect back. At $t = 8.5$, the wave pattern of the second shock/vortex interaction is shown in Fig. 8d. The R_2'' wave moves away from the spiral vortex V. The reflected shock R_1 is entering the duct. The kink K moves farther downstream. An enlarged plot of vorticity contours in a prescribed region is shown in Fig. 8e. From Fig. 8e, one can clearly see a small vortex V_1. An enlarged plot of pressure contours in a rectangular region containing the R_2'' wave is shown in Fig. 8f. It is found that there is an interlace phenomenon of high (+) and low (−) pressures. It is believed that this interlace of pressure distribution leads to the formation of AWs that propagate away from the spiral vortex.

IV. Conclusions

The problem of reflected-shock/spiral-vortex interactions has been investigated by using a high-resolution Euler solver, which is validated to be reasonably accurate. To analyze the complicated flowfields due to the shock/vortex interactions, computational shadowgraphs, computational schlieren images, and computational inteferometry are employed. Detailed flow structures of reflected-shock/spiral-vortex interactions are investigated for different incident shock Mach numbers. An interesting result of a stagnant reflected shock wave downstream of the duct is found for incident shock Mach numbers equal to or greater than the critical value of about 1.4. For the incident shock Mach number below the critical value, the reflected shock R_1 will eventually enter the duct. The mechanism for the formation of AWs generated by reflected-shock/spiral-vortex interactions in two-dimensional or axisymmetric cases is analyzed.

Acknowledgments

The support for this study under Grant NSC 91-2213-E006-107 is gratefully acknowledged. The authors thank B. Skews for reading the manuscript and comments.

References

[1]Skews, B. W., "The Perturbed Region Behind a Diffracting Shock Wave," *Journal of Fluid Mechanics*, Vol. 29, Pt. 4, 1967, pp. 705–719.

[2]Takayama, K., and Inoue, O., "Shock Wave Diffraction over a 90 Degree Sharp Corner–Posters Presented at 18th ISSW," *Shock Waves*, Vol. 1, No. 4, 1991, pp. 301–312.

[3]Yang, J., Kubota, T., and Zukoski, E. E., "An Analysis and Computational Investigation of Shock-Induced Vortical Flows," AIAA Paper 92-0316, Jan. 1992.

[4]Yates, L. A., "Images Constructed from Computed Flowfields," *AIAA Journal*, Vol. 31, No. 10, 1993, pp. 1877–1884.

[5]Sun, M., and Takayama, K., "The Formation of a Secondary Shock Wave Behind a Shock Wave Diffracting at a Convex Corner," *Shock Waves*, Vol. 7, No. 5, 1997, pp. 287–295.

[6]Kim, H. D., and Setoguchi, T., "Study of the Discharge of Weak Shocks from an Open End of a Duct," *Journal of Sound and Vibration*, Vol. 226, No. 5, 1999, pp. 1011–1028.

[7]Jiang, Z., and Takayama, K., "An Investigation into the Validation of Numerical Solutions of Complex Flowfields," *Journal of Computational Physics*, Vol. 151, No. 2, 1999, pp. 479–497.

[8]Szumoswki, A., Sobieraj, G., Selerowicz, W., and Piechna, J., "Starting Jet-Wall Interaction," *Journal of Sound and Vibration*, Vol. 232, No. 4, 2000, pp. 695–702.

[9]Inoue, O., and Hattori, Y., "Sound Generation by Shock-Vortex Interactions," *Journal of Fluid Mechanics*, Vol. 380, Feb. 1999, pp. 81–116.

[10]Chen, H., and Liang, S. M., "Planar Blast/Vortex Interaction and Sound Generation," *AIAA Journal*, Vol. 40, No. 11, 2002, pp. 2298–2304.

[11]Henderson, L. F., Vasillev, E. I., Ben-Dor, G., and Elperin, T., "The Wall-jetting Effect in Mach Reflection: Theoretical Consideration and Numerical Investigation," *Journal of Fluid Mechanics*, Vol. 479, March 2003, pp. 259–286.

[12]Sun, M., and Takayama, K., "Vorticity Production in Shock Diffraction," *Journal of Fluid Mechanics*, Vol. 478, March 2003, pp. 237–256.

[13]Jiang, G.-S., and Shu, C.-W., "Efficient Implementation of Weighted ENO Schemes," *Journal of Computational Physics*, Vol. 126, No. 1, 1996, pp. 202–228.

[14]Yang, J. M., "Experimental and Theoretical Study of Weak Shock Waves," Ph.D. Dissertation, Inst. of Fluid Science, Tohoku Univ., Sendai, Japan, April 1995, pp. 141–148.

[15]Thompson, W., "Time Dependent Boundary Conditions for Hyperbolic Systems," *Journal of Computational Physics*, Vol. 68, No. 1, 1987, pp. 1–24.

[16]Abate, G., and Shyy, W., "Dynamic Structure of Confined Shocks Undergoing Sudden Expansion," *Progress in Aerospace Sciences*, Vol. 38, No. 1, 2002, pp. 23–42.

[17]Kleine, H., Ritzerfeld, E., and Grönig, H., "Shock Wave Diffraction at a Ninety Degree Corner," *Computational Fluid Dynamics Journal*, Vol. 12, No. 2, Special Issue, 2003, pp. 142–158.

[18]Matsuo, K., Miyazato, Y., and Kim, H. D., "Shock Train and Pseudo-Shock Phenomena in Internal Gas Flows," *Progress in Aerospace Sciences*, Vol. 35, No. 1, 1999, pp. 33–100.

M. Sichel
Associate Editor